Stopped-Flow Fourier Transform Infrared Spectroscopy Allows Continuous Monitoring of Azide Reduction, Carbon Monoxide Inhibition, and ATP Hydrolysis by Nitrogenase†

John D. Tolland and Roger N. F. Thorneley*

Department of Biological Chemistry, John Innes Centre, Norwich NR4 7UH, U.K.

Received March 11, 2005; Revised Manuscript Received May 16, 2005

ABSTRACT: Stopped-flow FTIR spectroscopy was used to monitor continuously the pre-steady- and steady-state phases of azide reduction by nitrogenase and the accompanying hydrolysis of ATP. This was characterized by a ca. 1.3 s lag phase that is explained by the number of Fe protein cycles required to effect the reductions of azide to $N_2 + NH_3$, $N_2H_4 + NH_3$, or $3NH_3$. Extrapolation of the steady-state time course for azide reduction to zero time showed that one azide binds within 200 ms to each FeMo cofactor. Inhibition of azide reduction by CO was established at times <400 ms, which was faster than the appearance of the first observable IR band assigned to CO (1904 cm^{-1} detectable at ca. 1 s with maximum amplitude at ca. 7 s). IR bands associated with the rapidly formed (<400 ms) CO species that inhibits azide reduction were not observed over the range 1700−2100 cm^{-1}. This suggests either that the CO is initially bridging two or more Fe atoms or that a rapid reduction of CO to a formyl state occurs by insertion into a metal−hydride bond. The frequencies and time courses for the appearance and loss of the CO bands under hi- and lo-CO conditions were essentially unaffected by the presence of 20 mM azide, consistent with CO being a noncompetitive inhibitor of azide reduction and with azide and CO binding to different sites on the FeMo cofactor.

Nitrogenases isolated from diazotrophic bacteria (e.g., *Klebsiella pneumoniae* and *Azotobacter vinelandii*) catalyze the six-electron reduction of dinitrogen to ammonia with the concomitant two-electron reduction of protons to dihydrogen (*1*−*3*). Under optimum conditions in vitro, with sodium dithionite as the reductant, these eight-electron transfers and associated protonations are coupled to the hydrolysis of 16 MgATP. In addition to dinitrogen, there is a wide range of alternative reducible substrates that include alkynes, alkyl cyanides, and isocyanides and in the context of this paper azide. The structures of the Mo-containing nitrogenases have been determined at high resolution (*4*−*6*). They comprise two proteins, the Fe protein[1] and the MoFe protein (designated Kp2 and Kp1, respectively, in this study for the enzyme isolated from *K. pneumoniae*). Kp2 (γ_2) contains a single [4Fe-4S] cluster bound at the interface of the two identical subunits, each of which has an MgATP binding/hydrolysis site. The MoFe protein ($\alpha_2\beta_2$) has two types of unique metal clusters, with one of each cluster type in each $\alpha\beta$ dimer. The [8Fe-7S] P-cluster is located at the interface of the α and β subunits, and the [7Fe-9S-Mo-X-homocitrate] FeMo cofactor is buried in the α subunit. MgATP-dependent electron transfer proceeds within the Kp2−Kp1 protein complex from the 4Fe-4S cluster in Kp2 to the FeMo cofactor via the P-cluster in Kp1. Although it is now clear that the FeMo cofactor is the site of substrate binding and reduction, it is only recently that progress has been made in determining which of the eight metal ions and bridging sulfide ligands directly interact with a particular substrate or inhibitor (*7*−*11*). A major difficulty is the transient nature of the reduced states of the FeMo cofactor that bind and reduce substrates due to competing proton reduction to yield dihydrogen. In addition, there is currently no chemical agent that can access and reduce the FeMo cofactor. Reduction can only be achieved by electron transfer from the Fe protein accompanied by the hydrolysis of MgATP. Thus appreciable quasi-steady-state concentrations of intermediate forms of the FeMo cofactor with substrates, substrate-derived intermediates, or products bound can only be maintained over a period of seconds. Thus it is extremely unlikely that X-ray crystallography will be able to determine the structures of these intermediates that are so crucial to understanding the mechanism of nitrogenase. To date a combination of site-directed mutagenesis and EPR/ENDOR spectroscopy on frozen samples has been the most successful approach, a major advance being the identification of a cofactor-bound intermediate formed from the alkyne substrate propargyl alcohol (*8*, *12*) and very recently a protonated (dihydride) state of the cofactor (*11*). However, EPR-based techniques have two major limitations: they can only be applied to paramagnetic centers and they require frozen samples, which

† This work was supported by the UK Biotechnology and Biological Sciences Research Council through the Core Strategic Grant to the John Innes Centre and a Biomolecular Sciences Committee Studentship grant to J.D.T.

* To whom correspondence should be addressed. Tel: +44 1603 450739. Fax: +44 1603 40018. E-mail: Roger.thorneley@bbsrc.ac.uk.

[1] Abbreviations: EPR, electron paramagnetic resonance; Kp, *Klebsiella pneumoniae*; Fe protein, iron protein; MoFe protein, molybdenum iron protein; lo-CO, CO concentration stoichiometric with that of the FeMo cofactor; hi-CO, CO concentration of 500 μM; e^-, electron; SF-FTIR, stopped-flow Fourier transform infrared.

10.1021/bi050453m CCC: $30.25 © 2005 American Chemical Society
Published on Web 06/15/2005

precludes continuous monitoring. We have therefore been developing anaerobic stopped-flow FTIR spectroscopy to monitor in real time small molecule binding and activation at metal centers in enzymes such as nitrogenase (*13*), methane monooxygenase (*14*), and hydrogenase (*15*).

In the present paper we have extended our SF-FTIR studies on the binding of the inhibitor CO to functioning nitrogenase (*13*, *16*) to CO inhibition of azide reduction. Azide undergoes two-, six-, and eight-electron reductions to give dinitrogen, hydrazine, and ammonia as products (*10*, *17*):

$$N_3^- + 3H^+ + 2e^- \rightarrow N_2 + NH_3 \quad (1)$$

$$N_3^- + 7H^+ + 6e^- \rightarrow N_2H_4 + NH_3 \quad (2)$$

$$N_3^- + 9H^+ + 8e^- \rightarrow 3NH_3 \quad (3)$$

Of the species potentially present in solution and/or bound to the FeMo cofactor during turnover, N_3^- (2048 cm^{-1}), HN_3 (2146 cm^{-1}) and N_2 (end on metal bound 1800−2000 cm^{-1}) have IR bands that are relatively easy to monitor by SF-FTIR. At pH 7.4, hydrazoic acid ($pK_a = 4.6$) (*18*) is essentially completely dissociated with 99.9% present as the azide anion.

In addition to its intrinsic interest as a substrate, the reduction of azide is expected to proceed via intermediates bound at the FeMo cofactor that are common to those formed during dinitrogen reduction (e.g., Fe- or Mo-bound dinitrogen, diazinido, hydrazido 2−, nitrido) (*17*). Although we have not to date been able to detect azide-derived intermediates, we do report in this paper the first continuous direct monitoring of any substrate reduction by nitrogenase, the stoichiometry of azide binding to the FeMo cofactor, and the relationship between the site of azide binding and those of CO binding.

MATERIALS AND METHODS

Nitrogenase component proteins were purified from *K. pnuemoniae (oxytoca)* NCIB 12204 as previously described (*19*, *20*). The specific activities of Kp1 and Kp2 at 30 °C were 2200 and 1400 nmol of C_2H_4 produced min^{-1} (mg of protein)$^{-1}$, respectively. Metal analysis by ICPE spectroscopy gave a Mo content in the range of 1.1−1.4 ± 0.1 mol/mol of Kp1 protein.

Infrared spectra were measured at 4 cm^{-1} resolution on a modified Bruker IF66S spectrometer fitted with a liquid N_2 cooled mercury cadmium telluride (MCT) detector. The two-syringe stopped-flow drive system and IR cell have been described elsewhere (*13*, *21*). Narrow bandwidth filters 2170−1950, 2000−1800, 1750−1500, and 1600−980 cm^{-1} (Northumbria Optical Coatings, Tyne and Wear, U.K.), placed directly in front of the MCT detector, were used for the azide, CO, and ATP hydrolysis time courses. The drive system and thermostated IR cell with integral mixer were entirely located in an anaerobic and dry glovebox operated under N_2 with <2 ppm O_2 (Belle Technology, Portesham, Dorset, U.K.). The IR cell path length was calibrated to be 33 μm by fringe pattern analysis. FTIR peak intensity as a function of time was determined by fitting a time-averaged spectrum (Figure 1) to a sum of Voigt function line shapes. The peak widths and positions were then constrained, and

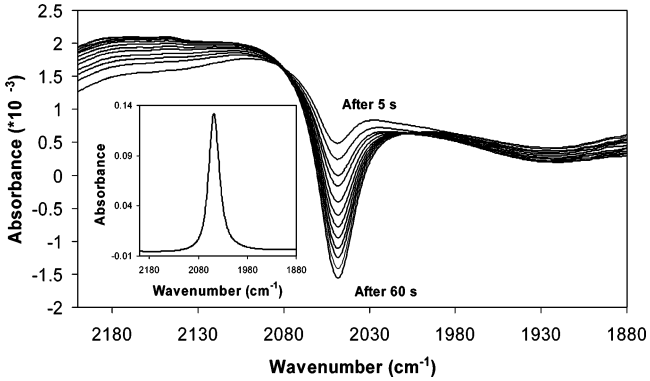

FIGURE 1: IR difference spectra in the region of the 2048 cm^{-1} azide band obtained at 5 s intervals during the reduction of azide by nitrogenase (20 mM azide, 10 μM Kp1, 40 μM Kp2). The time courses in Figures 2 and 8 were obtained by fitting similar spectra to a Voigt function as described in Materials and Methods. The insert shows a 20 mM azide spectrum, pH 7.4

for each spectrum of the time course, peak intensities and a baseline function were allowed to float. This approach significantly reduced the "noise" in the time course and eliminated any time-dependent baseline instabilities or contributions from other time-dependent changes. It also ensured that only changes in the specific band of interest were determined (*13*, *16*).

All experiments used 25 mM HEPES buffer, pH 7.4, containing 10 mM $MgCl_2$ and 10 mM sodium dithionite under 1 atm of argon unless stated. Background spectra were obtained by shooting, in turn, solutions of Kp2 + Kp1, MgATP + N_3^-, and MgATP + N_3^- + CO against this buffer. For data collection, syringe A usually contained Kp1 + Kp2 and syringe B MgATP + N_3^- (±CO). All salts and chemicals were purchased from Sigma (Poole, Dorset, U.K.) and high-purity CO was from BOC Gases (Guildford, U.K.).

Classical stopped assays were used to measure the hydrogen evolution and ATP hydrolysis rates during the quasi-steady-state period of azide reduction (10−40 s reaction times). These assays, designed to complement the IR studies, were performed under the same experimental conditions. Forty millimolar azide, 18 mM ATP, and 10 mM DT (0.2 mL) were injected into each of three preweighed argon-flushed 7.8 mL assay vials, fitted with rubber closures. These were then equilibrated to 23 °C in a shaking water bath. The reactions were then initiated by the addition of 0.2 mL of a 20 μM Kp1, 80 μM Kp2, and 10 mM DT protein mix, also preequilibrated to 23 °C. The final reaction concentrations were thus 10 μM Kp1, 40 μM Kp2, 20 mM azide, 9 mM MgATP, and 10 mM DT. A minimum of five assays at each incubation time were performed. Reaction termination was by the addition of 0.3 mL of 0.4 M EDTA, pH 7.5. The short times were possible by having the syringe containing the EDTA already inserted into the "Suba-seal" rubber closure at the commencement of the assay. Great care was taken to ensure that no contamination of the assay mixture occurred. Controls involved the addition of 0.3 mL of 0.4 M EDTA to the reaction mixture prior to protein addition. After the assays were stopped, they were placed on ice to minimize any further hydrolysis of ATP or ADP. Dihydrogen production was measured on a Shimadzu GC-14B gas chromatograph fitted with a thermal conductivity detector (Katharometer), with argon as the carrier gas essentially as

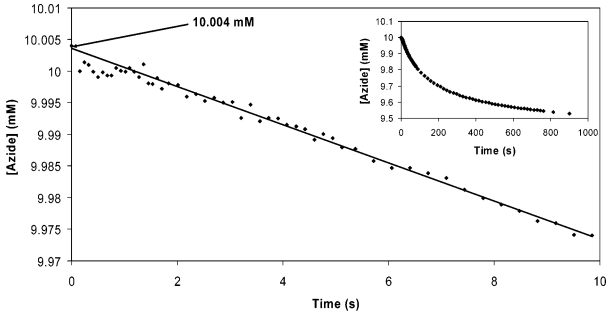

FIGURE 2: First 10 s of the time course for the reduction of 10 mM azide by 10 μM Kp1 and 40 μM Kp2 showing a 1.3 s lag phase. The difference between the ordinate intercept of the extrapolated steady-state time course and the constant azide concentration measured during the 1.3 s lag phase was used to calculate a 1:1 stoichiometry for azide binding to FeMo cofactor. The insert shows the full time course with the onset of inhibition due to exhaustion of MgATP and the accumulation of MgADP. The data are the mean of eight experiments.

previously described (*17*). Ammonia was determined by the indophenol method (*22*), hydrazine as a *p*-dimethylaminobenzaldehyde adduct (*17*), and phosphate by the method of Ottolenghi (*23*).

RESULTS AND DISCUSSION

Azide Reduction. The insert to Figure 1 shows the 2048 cm^{-1} IR band that can be used to monitor in real time the kinetics of azide reduction by nitrogenase. Figure 1 shows time-averaged difference spectra (5 s integration time) taken at 5 s intervals (5−60 s) using the 20 mM azide spectrum as a reference. These negative amplitudes represent the amount of azide anion that has been reduced by nitrogenase at each time point. These initial difference spectra confirmed the feasibility of using IR spectroscopy to continuously monitor in real time substrate reduction by nitrogenase. Previously, all nitrogenase substrate reduction kinetic studies have used stopped assays followed by mass spectrometric or chemical analysis. The insert to Figure 2 shows a time course (150 ms to 900 s) over which time ca. 500 μM of the 10 mM azide initially present has been reduced by nitrogenase. The rate of azide reduction declines significantly at times greater than ca. 30 s due to the hydrolysis of MgATP and accumulation of the inhibitor MgADP (the direct monitoring by SF-FTIR of MgATP hydrolysis concomitant with azide is described below). Figure 2 shows that over the period 1.5−10 s the rate of azide reduction is essentially constant and that a steady state has been attained. The rate of azide reduction was determined at six azide concentrations in the range 1.0−20 mM with 10 μM Kp1 and 40 μM Kp2. An apparent $K_m = 9.1 \pm 0.2$ mM, $V_{max} = 7.7 \pm 0.05$ μM s^{-1}, and $k_{cat} = 0.7 \pm 0.07$ s^{-1} (based on 1.1 ± 0.1 mol of Mo/mol of Kp1) were obtained after fitting to the Michaelis−Menten equation (Figure 3). The apparent K_m determined by SF-FTIR is significantly higher than that previously reported for the reduction of azide to ammonia (1.3 mM) and azide to hydrazine (3.3 mM) using stopped assays and product analysis (*17*). The Lowe−Thorneley scheme predicts that the K_m for substrates will depend on both the ratio and absolute concentration of nitrogenase proteins (*24*). The previous values of apparent K_m for azide reductions to ammonia and hydrazine were determined at ca. 50-fold lower nitrogenase protein concentrations (e.g., 0.2 μM Kp1; cf. 10 μM Kp1 for these SF-FTIR experiments) in stopped assays run at 30 °C (cf. 23 °C for SF-FTIR). The higher protein concentration and the temperature difference are the most likely explanations for the higher apparent K_m value determined by SF-FTIR. In fact, the high protein concentrations necessary for SF-FTIR studies (ca. 50 μM active sites for single turnover and 10 μM for steady-state experiments) are more relevant to the in vivo situation when ca. 10% of the soluble protein in diazotrophs is present as nitrogenase under nitrogen-fixing conditions with a ca. 3:1 ratio of Fe:MoFe protein. These high protein concentrations improve the efficiency of nitrogenase with respect to minimizing H_2 production and maximizing N_2 reduction (*25*).

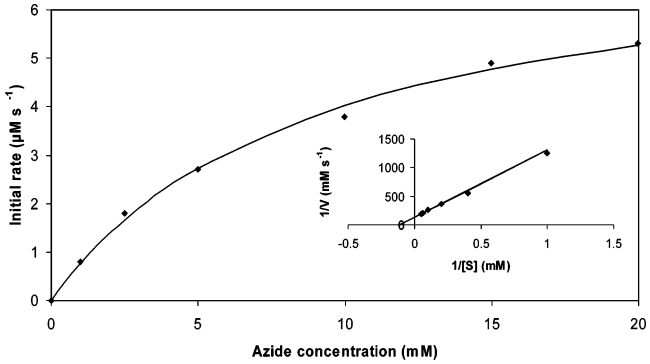

FIGURE 3: Plot of initial rate of azide reduction (over 2−8 s) against azide concentration. The solid line is a fit generated using the Michaelis−Menten equation ($v_0 = V_{max}[S]/K_m + [S]$). Insert: Lineweaver−Burk plot of the data. The solid line is a linear least-squares fit generated using the Michaelis−Menten equation.

The turnover time of 1.4 ± 0.14 s is consistent with the observed lag phase of ca. 1.3 s for azide reduction seen in Figure 2, provided the initial binding of azide to the FeMo cofactor occurs at times <200 ms, which is the time resolution limit for this SF-FTIR study. Support for this assumption comes from pre-steady-state rapid acid quench data for ammonia and hydrazine formation from azide reduction, which show lag phases of 80 ± 20 and 180 ± 20 ms, respectively (*17*). These rapid acid quench data were obtained at 23 °C with protein concentrations (15 μM Kp1, 75 μM Kp2) comparable to those used in the SF-FTIR studies. Clearly, before any ammonia can be released, even on acid quenching, azide must first bind to the FeMo cofactor that is at least one-electron reduced since no product was detected on acid quenching azide in the presence of enzyme in the absence of MgATP. Thus the data in Figure 2 can be used to calculate the stoichiometry of azide binding to the reduced FeMo cofactor. Extrapolation of the linear initial steady-state phase (2−10 s) back to zero time shows that 4 μM azide binds rapidly to the Kp1 in a reaction that is too fast to observe by SF-FTIR (<200 ms). Since the apparent $K_m = 9.1$ mM, with 10 mM azide, the fraction of the FeMo cofactor that is bound by azide, assuming 1:1 stoichiometry, can be calculated as $10/[10 + 9.1] = 0.52$. Since the [FeMo cofactor] = 11 μM, this would require 5.7 μM azide to bind rapidly. This compares with a value of 4 μM obtained by extrapolating the data in Figure 2. A similar extrapolation of data obtained with 20 mM azide (Figure 8) gave 6 μM as the concentration of the rapidly bound azide, which compares with 7.6 μM calculated from the apparent K_m. We conclude that one azide molecule binds to the FeMo cofactor.

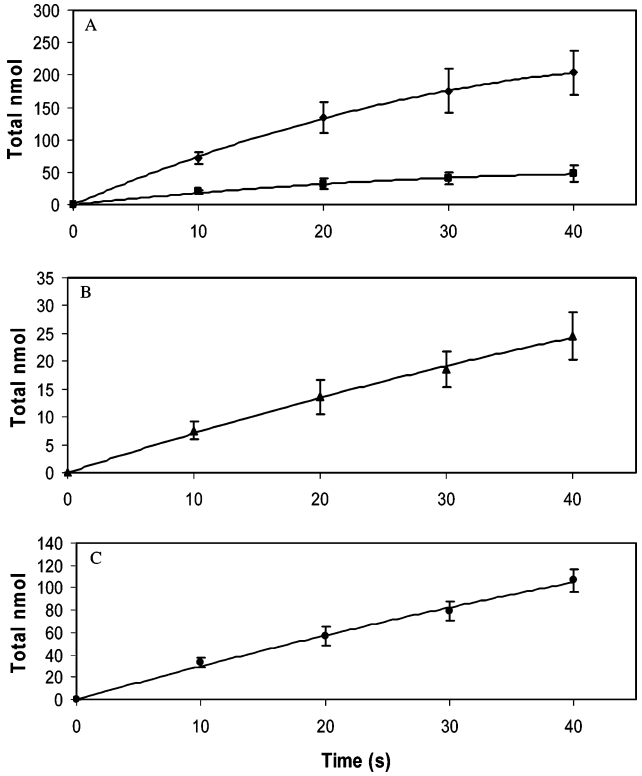

FIGURE 4: Total nanomoles of H_2 (A, ■), N_2H_4 (B), and NH_3 (C) formed from the reduction of 20 mM azide by 10 μM Kp1, 40 μM Kp2, 9 mM MgATP, and 10 mM DT. In the absence of azide only H_2 is produced (A, ◆).

To understand the mechanistic significance of the observed lag phase of the ca. 1.3 s for azide reduction, it was necessary to determine the product distribution (hydrazine, ammonia, and dihydrogen) in stopped assays run under the same conditions as those for the continuous monitoring of azide reduction by SF-FTIR. Panels A, B, and C of Figure 4 show time courses (10−40 s) for H_2 (±azide), hydrazine, and ammonia formation, respectively. The data in Figure 4A show that the rate of H_2 production decreases from 7.15 to 1.95 nmol s^{-1} in the presence of 20 mM azide. These rates were measured over the period 10−20 s when the effects of lag and burst phases and the onset of inhibition due to MgADP accumulation are minimal. Assuming that in the presence of azide the electron flux stays constant, 7.15 − 1.95 = 5.2 electron pairs s^{-1} were used to reduce azide i.e., 73% of the total electron flux [cf. 80% found previously (*17*)]. To calculate how these electron pairs are distributed across the two-, six-, and eight-electron reductions shown in eqs 1−3, it is ideally necessary to measure independently the rates of ammonia, hydrazine, and dinitrogen reduction as previously done (*17*). In the present study it was not possible to measure dinitrogen production due to lack of appropriate mass spectrometry facilities. However, good estimates of the relative contributions of the two- and eight-electron reduction pathways can be made from the ammonia and hydrazine data shown in Figure 4B,C. Hydrazine and ammonia were produced at rates of 0.75 and 3.3 nmol s^{-1}, respectively. Thus eq 2 is responsible for 3 × 0.75 = 2.2 electron pairs s^{-1} leaving 5.2 − 2.2 = 3.0 electron pairs s^{-1} to be distributed between eqs 1 and 3 for the production of 3.3 − 0.75 = 2.55 nmol s^{-1} of the remaining ammonia. A 50% distribution of this ammonia between eqs 1 and 3 would require precisely the 3 electron pairs s^{-1} available assuming constant electron flux. Thus the percentages of the electron flux used for azide reduction for the two-, six-, and eight-electron reductions are 25% (eq 1), 43% (eq 2), and 32% (eq 3). These compare with values of 22%, 32%, and 46% reported previously (*17*) using ca. 50-fold lower protein concentrations at 30 °C. These kinetic data for product formation/distribution equate to a rate of azide consumption of 6.2 μM s^{-1}, which compares well with the rate of 5.3 μM s^{-1} measured directly by SF-FTIR.

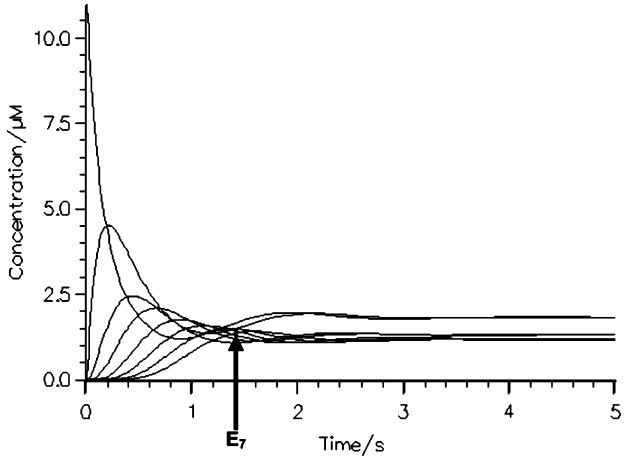

FIGURE 5: Lowe−Thorneley simulation of the concentration of Kp1 in states E_0 through E_7. The simulation was run using the same reactant concentrations as in the text, i.e., 10 μM Kp1, 40 μM Kp2, 9 mM MgATP, and 10 mM DT. The rate constants that were used for these simulations were those used previously by Thorneley and Lowe for N_2 reduction (*24*, *34*, *35*). The reduction of N_2 to $2NH_3 + H_2$ also requires an eight-electron cycle as does the reduction of N_3^- to $3NH_3$. The arrow shows the maximum amplitude of E_7 at 1.4 s, which corresponds closely to the observed lag phase for azide reduction.

Figure 5 shows simulated time courses for each of the states E_0 through E_7 of Kp1 using the Lowe−Thorneley (*34*, *35*) scheme with the protein concentrations used in the SF-FTIR and stopped-assay experiments described above. The rate constants used in these simulations were those determined previously for N_2 reduction (*24*). The lag phase in azide reduction (ca. 1.3 s) and the turnover time (1.4 s) calculated from the steady-state rate of azide consumption are consistent with the measured distribution of the electron flux used to reduce azide i.e., 43% into the six-electron reduction (eq 2) and 33% into the eight-electron reduction (eq 3). As shown by the simulations in Figure 5, lag phases of the order of ca. 1 s are consistent with the Kp1 species E_6 and E_7 being generated during the catalytic cycle for azide reduction. A high percentage of the Kp1 must pass through states E_6 and E_7, presumably with azide reduction intermediates/products bound before a second reductive cycle with a second azide molecule can commence. This is consistent with rapid acid quench data for ammonia formation from azide that showed a burst phase of ca. 1 s duration prior to establishment of a steady state (*17*).

A complicating factor in interpreting the duration of the lag phase for azide reduction is the concomitant evolution of H_2. Under the conditions of the SF-FTIR and stopped-assay experiments ca. 27% of the total electron flux is used to reduce protons to dihydrogen. This is due in part to only 70% saturation of the azide binding site based on the K_m of

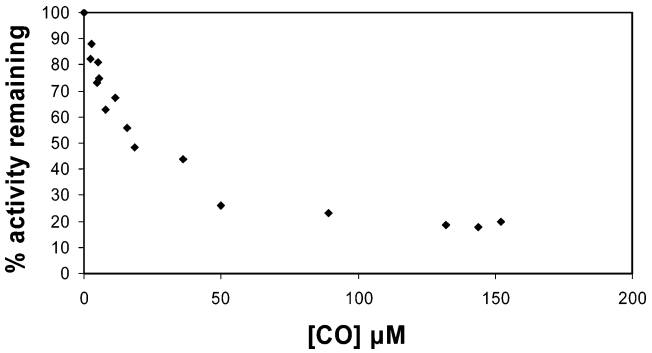

FIGURE 6: Dependence of the steady-state rate of azide reduction of nitrogenase on increasing CO concentration. The plot is of the initial rate of loss of the 2048 cm^{-1} azide band, taken over 2−8 s, expressed as a percentage of the activity in the absence of CO. Present: 10 μM Kp1, 40 μM Kp2, 20 mM NaN_3, 9 mM ATP, and 10 mM DT.

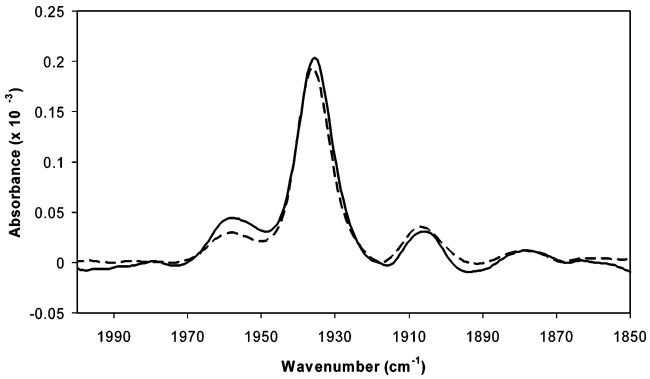

FIGURE 7: Comparison of the hi-CO bands in the presence (—) and absence (− −) of 20 mM azide: presence of azide, 30 μM Kp1 and 100 μM Kp2; absence of azide, 50 μM Kp1 and 150 μM Kp2. The amplitudes of the spectra have been normalized to the same molybdenum concentration.

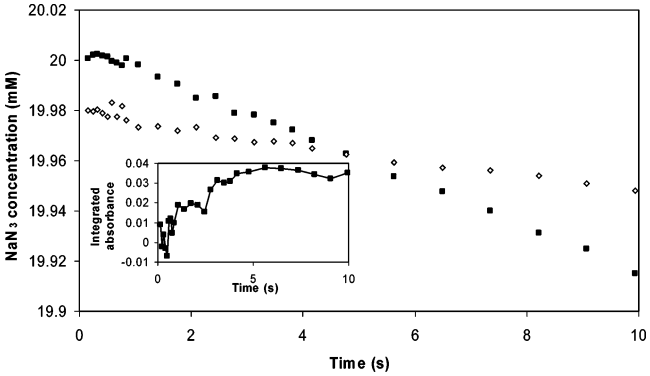

FIGURE 8: Inhibition of azide reduction by CO. Time courses for the reduction of 20 mM azide by 10 μM Kp1 and 40 μM Kp2 in the absence (■) and presence (◇) of stoichiometric CO. The CO-inhibited time course has been offset by 0.02 mM azide for clarity. Insert: the lo-CO 1904 cm^{-1} time course under the same conditions showing essentially a zero amplitude at 1s and a maximum amplitude at ca. 7 s; i.e., CO inhibition of azide reduction is fully established before the appearance of the 1904 cm^{-1} CO band.

9 mM with 20 mM azide in solution. In addition, the data of Dilworth and Thorneley (*17*), albeit at lower protein concentrations and at 30 °C, showed that, even at an azide concentration extrapolated to infinity, at pH 7.4 ca. 15% of the electron flux is still used to reduce protons. However, complete suppression of hydrogen evolution, calculated from the extrapolation of the dependence of hydrogen evolution rates on azide concentration at pH 8.2, showed that hydrogen production is not an integral part of azide reduction (*17*). The effect of competing hydrogen evolution will be to extend the lag phase prior to attainment of a quasi-steady-state rate of azide reduction consistent with the observed lag phase of ca. 1.3 s.

CO Inhibition of Azide Reduction. Figure 6 shows the effect of increasing concentrations of CO on the steady-state rate of azide reduction measured by SF-FTIR over the time interval 2−8 s. Fifty percent inhibition was observed with 20 μM CO. These data are consistent with the steady-state data obtained at lower protein concentrations and at 30 °C by Dilworth and Thorneley (*17*), which gave $K_{is} = 1.2$ μM and $K_{ii} = 24$ μM for CO as a noncompetitive inhibitor of azide reduction with respect to both hydrazine and ammonia as products. Further evidence for azide and CO binding to different sites is that the frequencies and intensities of the hi-CO bands at 1958, 1936, 1906, and 1880 cm^{-1} and the lo-CO band at 1904 cm^{-1} were essentially unaffected by the presence of 20 mM azide (Figure 7). Azide (20 mM) had little or no effect on the time courses for the appearance and disappearance of these bands (data not shown), which were very similar to those published previously in the absence of azide (*16*). Since ENDOR studies have established CO binding to Fe (*26*), these data cause us not to exclude Mo as the site of azide reduction.

Figure 8 shows the inhibition of the rate of azide reduction by lo-CO (stoichiometric with the FeMo cofactor) over the first 10 s of reaction. In the absence of CO, a lag phase of 1.3 s (also shown in Figure 2 and discussed above) is apparent before a steady-state rate of azide reduction of 8.5 μM s^{-1} is established. This rate is comparable to that calculated from the data in Figure 2 (5.3 μM s^{-1}), after correction for the differing Mo contents (1.4 and 1.1 ± 0.1 mol of Mo/mol of Kp1). In the presence of lo-CO the steady-state rate decreases by 56% to 3.7 μM s^{-1}. This inhibition is comparable with the 57% previously reported (*17*). What is of particular interest is that the CO-inhibited rate of azide reduction is established at times <1 s. The lo-CO 1904 cm^{-1} IR band, the first to appear, is barely detectable at 1 s (Figure 8 insert), not reaching its maximum intensity until ca. 7 s. Thus the rapid onset of the inhibition of azide reduction by CO does not correlate with the slow appearance of the 1904 cm^{-1} CO band. Further evidence for the fast (<1 s) onset of CO inhibition of substrate reduction comes from published rapid acid quench data for CO inhibition of acetylene reduction to ethylene (*27*). The rate of ethylene formation was >80% inhibited by 5% CO at times <400 ms. As shown in Figure 7, 20 mM azide does not perturb any of the CO bands observed to date. Therefore, the IR band associated with the rapidly binding CO responsible for inhibiting azide reduction at times <1 s has yet to be identified. We have looked unsuccessfully for this band at short times in the frequency range 1700−2000 cm^{-1}, the fastest forming CO band observed being at 1904 cm^{-1}, which takes ca. 7 s to reach its maximum amplitude (insert to Figure 8). We conclude that the CO responsible for the rapid inhibition of azide reduction has an IR band at an unusually low frequency due to either bridging between Fe atoms and/or reduction to a formyl-type ligand. Precedents for this type of chemistry are model complexes of the diiron center in hydrogenase. A

band at 1741 cm^{-1} which shifts to 1670 cm^{-1} on ion pairing with Li^+ in THF has been assigned to the bridging CO in $[Fe_2(\mu\text{-}S)(CH_2)_3SH(\mu\text{-}CO)(CO)_6]^-$ (*28*). In the same paper a band at 1555 cm^{-1}, appearing on reduction with Li[$HBEt_3$], was assigned to the terminal formyl in $[Fe_2(\mu\text{-pdt})(CHO)(CO)_5]^-$ (pdt = propane-1,3-dithiolate). In the context of this paper, it is relevant that the terminal formyl derivative converted to the bridging CO compound in a reaction whose rate was dependent on the free CO concentration in solution and the redox potential.

IR spectroelectrochemical studies on isolated FeMo cofactor under lo-CO conditions detected a transient IR band at 1835 cm^{-1} that converted to an 1808 cm^{-1} band following a one-electron reduction. These bands were assigned to a single CO in a bridging mode between two central Fe atoms (*29*). Further reduction under hi-CO resulted in the loss of the 1808 cm^{-1} band and the appearance of two new IR bands at 1885 and 1920 cm^{-1}, assigned to two terminally bound CO on two central Fe atoms and a third CO at Mo. In our SF-FTIR studies on functioning nitrogenase both in the absence (*16*) and in the presence of azide (this study) under hi-CO, we have observed CO bands at 1958, 1936, 1904, and 1880 cm^{-1} (Figure 7). At long times (>200 s) these bands are replaced by a low-frequency band at 1715 cm^{-1} (*16*). We have never observed a band in the region of 1808 cm^{-1}. It is possible that the 1715 cm^{-1} band that grows in at the expense of the higher frequency bands as the redox potential rises due to exhaustion of MgATP and accumulation of MgADP is a bridging CO analogous to the 1808 cm^{-1} band of isolated cofactor but shifted by ca. 100 cm^{-1} due to the protein environment of the cofactor in functioning nitrogenase. A hydrogen bond between the ketonic oxygen of a bridging CO and adjacent amino acid side chains (e.g., His 195) would be expected to significantly shift the carbonyl band to lower frequencies. Such is the unique chemistry carried out by the FeMo cofactor in nitrogenase that the rapid transient formation of the bridging formyl (*30*) or terminal thiocarbonyl (Fe−SCHO with the sulfur coming from a μ-S^{2-} in the FeMo cofactor) (*31*) species merit consideration and could usefully be subjected to DF theory analysis. The detection of the low-frequency IR bands characteristic of these species would be very difficult due to the requirement of working in D_2O and the strong absorbance of the protein amide bands in the region 1700−1500 cm^{-1}. Direct evidence for the formation of Fe hydride species comes from recent ENDOR studies when a sample of an α-70Ile variant MoFe protein was manually frozen after 20 s turnover under argon (*11*). It will be extremely interesting to rapid-freeze an ENDOR sample at ca. 200 ms under hi-CO/Ar in order to detect any formyl species formed by insertion of ^{13}CO into an Fe−H bond.

Direct Monitoring of ATP Hydrolysis Coupled to the Reduction of Azide. Figure 9 shows the IR spectra of MgATP, MgADP, MgAMP, and P_i under the conditions of the experiments described above. The hydrolysis of MgATP and formation of P_i that is coupled to azide reduction and concomitant hydrogen evolution were measured continuously by SF-FTIR at 1248 and 1086 cm^{-1}, respectively. Figure 10 shows the time courses for loss of ATP and formation of P_i with initial rates over the first 10 s reaction time of 111 μM s^{-1}. This value is very close to the rate of 108 μM s^{-1} determined using stopped assays followed by P_i determination by the spectrophotometric method of Ottolenghi (*23*) (Figure 11). The data in Figure 11 for assays in the presence and absence of azide (20 mM) and in the presence of azide (20 mM) plus hi-CO (500 μM) show that within experimental error the rate of ATP hydrolysis is constant. Under these conditions in the absence of azide and/or CO, the rate of hydrogen production was 17.9 μM s^{-1}, which with a rate of ATP hydrolysis of 111 μM s^{-1} from the SF-FTIR determination gives an ATP:2e^- of 6.2. The deviation of this value from the limiting ATP:2e value of 4.0 can be explained by

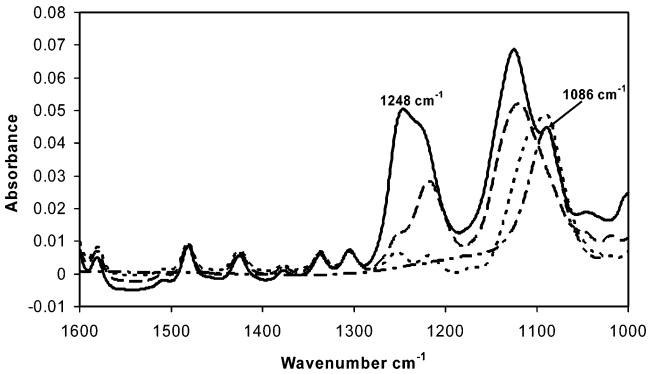

FIGURE 9: IR spectra of adenosine nucleotides (9 mM) and inorganic phosphate (9 mM): MgATP (—), MgADP (− −), MgAMP (· · ·), and P_i (− · −).

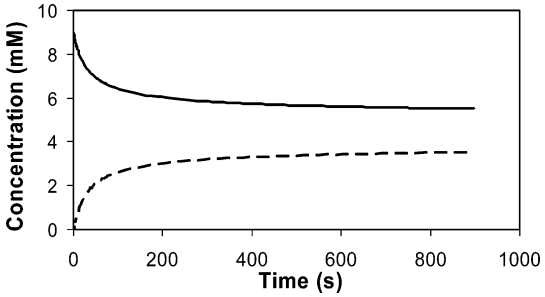

FIGURE 10: Time courses for nitrogenase-catalyzed hydrolysis of MgATP coupled to azide reduction obtained by direct monitoring of the loss of MgATP at 1248 cm^{-1} (—) and appearance of P_i at 1086 cm^{-1} (− −). Conditions at the start of the reaction: 10 μM Kp1, 40 μM Kp2, 20 mM NaN_3, 9 mM ATP, and 10 mM sodium dithionite.

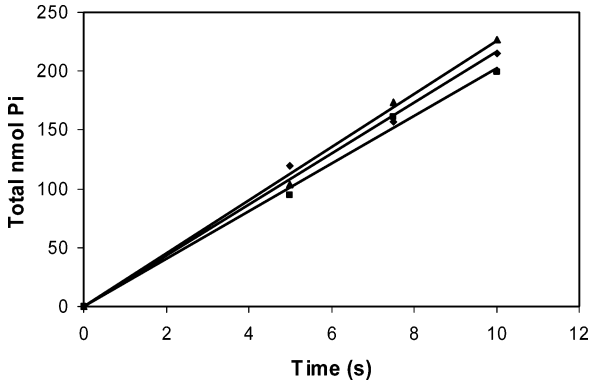

FIGURE 11: Stopped, conventional spectrophotometric assays for the total nanomoles of P_i produced by nitrogenase-catalyzed MgATP hydrolysis in the absence of azide (◆), the presence of 20 mM azide (■), and the presence of 20 mM azide and hi-CO (▲). These assays were done to validate the SF-FTIR data shown in Figure 10. Solid lines are linear least-squares fits. Present in all cases: 10 μM Kp1, 40 μM Kp2, 9 mM MgATP, and 10 mM sodium dithionite.

the high protein concentrations used in these experiments. According to the Lowe−Thorneley scheme with dithionite as reductant, high protein concentrations while optimizing dinitrogen reduction with respect to hydrogen evolution also increase the steady-state concentration of the complex formed between oxidized Fe protein with 2 MgADP bound and MoFe protein in states E_0 to E_7 (bottom right-hand corner of the Fe protein cycle). This complex is responsible for reductant-independent ATPase activity (*32*) and accounts for the uncoupling of ATPase activity from electron transfer.

CONCLUSIONS

Stopped-flow FTIR (SF-FTIR) spectroscopy has been used to monitor continuously the pre-steady- and steady-state phases of substrate (azide) reduction by nitrogenase. This is the first time that this has been achieved for any one of the many alternative substrates that are reduced by nitrogenase.

SF-FTIR has also been used to monitor continuously the concomitant hydrolysis of ATP that is coupled to the reduction of all substrates including azide. This allows the facile determination of the ATP:2e ratio that is the accepted measure of the efficiency of coupling of electron flux to ATP hydrolysis. Although not demonstrated in this paper, SF-FTIR offers the possibility of monitoring MgATP, MgADP, and P_i bound to transient forms for the Fe protein both in the Fe−MoFe protein complex and to the free forms of oxidized and reduced Fe protein. Clearly, the continuous direct monitoring of ATP hydrolysis rates by SF-FTIR has many potential applications with enzyme systems other than nitrogenase.

The reduction of azide was characterized by a ca. 1.3 s lag phase that is explained by the number of Fe protein cycles required to effect the two-, six-, and eight-electron reductions of azide to $N_2 + NH_3$, $N_2H_4 + NH_3$, and $3NH_3$, respectively. The percentage of the total electron flux used for each of these reductions and concomitant H_2 production is consistent with the observed lag phase. Extrapolation of the steady-state time course for azide reduction to zero time is consistent with one azide binding to each FeMo cofactor. This reaction occurs within the 200 ms time resolution of these experiments. This is the first time that the stoichiometry for reducible substrate binding to the FeMo cofactor in functioning nitrogenase has been determined.

Inhibition of azide reduction by CO was fully established at times <400 ms, which is much faster than the appearance of the 1904 cm^{-1} IR band assigned to CO (detectable at ca. 1 s with maximum amplitude at ca. 7 s). An IR band associated with the rapidly formed (<400 ms) CO species that inhibits azide reduction has not been observed over the range 1700−2100 cm^{-1}. This could indicate that the CO is in a multiple bridged environment that greatly decreases the C≡O bond order or that a rapid reduction of CO to a formyl (−CHO) species occurs. Since there are no data in the literature to suggest that CO can be reduced by nitrogenase and the product released, any transient species such as M−CHO would have to release CO as the FeMo cofactor reverted to state E_0 (Lowe−Thorneley nomenclature) on reductant and/or ATP exhaustion.

The frequencies and time courses for the appearance and loss of the CO bands under hi- and lo-CO conditions were essentially unaffected by the presence of 20 mM azide, consistent with CO being a noncompetitive inhibitor of azide reduction and with azide and CO binding to different sites on the FeMo cofactor. Since it is unlikely that azide and CO could bind simultaneously to the same metal ion without affecting the CO IR band(s), we conclude that CO and azide bind to different metal ions in the FeMo cofactor. EPR/ENDOR data have convincingly shown that CO binds to one (lo-CO) or two Fe atoms (hi-CO) (*26*); azide must therefore bind to either a third Fe atom or to the Mo, possibly by displacing the carboxylate ligand of homocitrate (*33*).

ACKNOWLEDGMENT

We appreciate the technical assistance of Gill Ashby and discussions with Simon J. George regarding the analysis of SF-FTIR data.

REFERENCES

1. Burgess, B. K., and Lowe, D. J. (1996) Mechanism of molybdenum nitrogenase, *Chem. Rev. 96*, 2983−3011.
2. Igarashi, R. Y., and Seefeldt, L. C. (2003) Nitrogen fixation: The mechanism of the Mo-dependent nitrogenase, *Crit. Rev. Biochem. Mol. Biol. 38*, 351−384.
3. Seefeldt, L. C., Dance, I. G., and Dean, D. R. (2004) Substrate interactions with nitrogenase: Fe versus Mo, *Biochemistry 43*, 1401−1409.
4. Mayer, S. M., Lawson, D. M., Gormal, C. A., Roe, S. M., and Smith, B. E. (1999) New insights into structure−function relationships in nitrogenase: A 1.6 Å resolution X-ray crystallographic study of *Klebsiella pneumoniae* MoFe-protein, *J. Mol. Biol. 292*, 871−891.
5. Kim, J., Woo, D., and Rees, D. C. (1993) X-ray crystal structure of the nitrogenase molybdenum−iron protein from *Clostridium pasteurianum* at 3.0 angstrom resolution, *Biochemistry 32*, 7104−7115.
6. Einsle, O., Tezcan, F. A., Andrade, S. L. A., Schmid, B., Yoshida, M., Howard, J. B., and Rees, D. C. (2002) Nitrogenase MoFe-protein at 1.16 angstrom resolution: A central ligand in the FeMo-cofactor, *Science 297*, 1696−1700.
7. Barney, B. M., Igarashi, R. Y., Dos Santos, P. C., Dean, D. R., and Seefeldt, L. C. (2004) Substrate interaction at an iron-sulfur face of the FeMo-cofactor during nitrogenase catalysis, *J. Biol. Chem. 279*, 53621−53624.
8. Igarashi, R. Y., Dos Santos, P. C., Niehaus, W. G., Dance, I. G., Dean, D. R., and Seefeldt, L. C. (2004) Localization of a catalytic intermediate bound to the FeMo-cofactor of nitrogenase, *J. Biol. Chem. 279*, 34770−34775.
9. Dance, I. (2004) The mechanism of nitrogenase. Computed details of the site and geometry of binding of alkyne and alkene substrates and intermediates, *J. Am. Chem. Soc. 126*, 11852−11863.
10. Fisher, K., Dilworth, M. J., and Newton, W. E. (2000) Differential effects on N_2 binding and reduction, HD formation, and azide reduction with alpha-195^{His} and alpha-191^{Gln}-substituted MoFe-proteins of *Azotobacter vinelandii* nitrogenase, *Biochemistry 39*, 15570−15577.
11. Igarashi, R. Y., Laryukhin, M., Dos Santos, P. C., Lee, H. I., Dean, D. R., Seefeldt, L. C., and Hoffman, B. M. (2005) Trapping H^- bound to the nitrogenase FeMo-cofactor active site during H-2 evolution: Characterization by ENDOR spectroscopy, *J. Am. Chem. Soc. 127*, 6231−6241.
12. Lee, H. I., Igarashi, R. Y., Laryukhin, M., Doan, P. E., Dos Santos, P. C., Dean, D. R., Seefeldt, L. C., and Hoffman, B. M. (2004) An organometallic intermediate during alkyne reduction by nitrogenase, *J. Am. Chem. Soc. 126*, 9563−9569.
13. Thorneley, R. N. F., and George, S. J. (2000) in *Prokaryotic Nitrogen Fixation: A model system for analysis of a biological process*, pp 81−89, Horizon Scientific Press, Wymondham, U.K.
14. Muthusamy, M., Ambundo, E. A., George, S. J., Lippard, S. J., and Thorneley, R. N. F. (2003) Stopped-flow Fourier transform infrared spectroscopy of nitromethane oxidation by the diiron-(IV) intermediate of methane monooxygenase, *J. Am. Chem. Soc. 125*, 11150−11151.
15. George, S. J., Kurkin, S., Thorneley, R. N. F., and Albracht, S. P. J. (2004) Reactions of H-2, CO, and O-2 with active NiFe-

hydrogenase from *Allochromatium vinosum*. A stopped-flow infrared study, *Biochemistry 43*, 6808−6819.
16. George, S. J., Ashby, G. A., Wharton, C. W., and Thorneley, R. N. F. (1997) Time-resolved binding of carbon monoxide to nitrogenase monitored by stopped-flow infrared spectroscopy, *J. Am. Chem. Soc. 119*, 6450−6451.
17. Dilworth, M. J., and Thorneley, R. N. F. (1981) Nitrogenase of *Klebsiella pneumoniae*: hydrazine is a product of azide reduction, *Biochem. J. 193*, 971−983.
18. Boughton, J. H., and Keller, R. N. (1966) Dissociation constants of hydropseudohalic acids, *J. Inorg. Nucl. Chem. 28*, 2851−2856.
19. Eady, R. R., Smith, B. E., Cook, K. A., and Postgate, J. R. (1972) Nitrogenase of *Klebsiella pneumoniae*: Purification and properties of the component proteins, *Biochem. J. 128*, 655−675.
20. Hino, S., and Wilson, P. W. (1958) Nitrogen fixation by a facultative *Bacillus*, *J. Bacteriol. 75*, 403−408.
21. White, A. J., Drabble, K., and Wharton, C. W. (1995) A stopped-flow apparatus for infrared spectroscopy of aqueous solutions, *Biochem. J. 306*, 843−849.
22. Dilworth, M. J., and Fisher, K. (1998) Elimination of creatine interference with the indophenol measurement of NH_3 produced during nitrogenase assays, *Anal. Biochem. 256*, 242−244.
23. Ottolenghi, P. (1975) The reversible delipidation of a solubilised sodium-plus-potassium ion-dependent adenosine triphosphatase from the salt gland of the spiny dogfish, *Biochem. J. 151*, 61−66.
24. Lowe, D. J., and Thorneley, R. N. F. (1984b) The mechanism of *Klebsiella pneumoniae* nitrogenase action: The determination of rate constants for the simulation of the kinetics of N_2 reduction and H_2 evolution, *Biochem. J. 224*, 895−901.
25. Thorneley, R. N. F., and Lowe, D. J. (1985) in *Molybdenum Enzymes* (Spiro, T. G., Ed.) pp 221−284, John Wiley and Sons, New York.
26. Lee, H. I., Cameron, L. M., Hales, B. J., and Hoffman, B. M. (1997) CO binding to the FeMo-cofactor of CO-inhibited nitrogenase: C-13 and H-1 Q-band ENDOR investigation, *J. Am. Chem. Soc. 119*, 10121−10126.
27. Lowe, D. J., Fisher, K., and Thorneley, R. N. F. (1990) *Klebsiella pneumoniae* nitrogenase: Mechanism of acetylene reduction and its inhibition by carbon monoxide, *Biochem. J. 272*, 621−625.
28. Borg, S. J., Behrsing, T., Best, S. P., Razavet, M., Liu, X. M., and Pickett, C. J. (2004) Electron transfer at a dithiolate-bridged diiron assembly: Electrocatalytic hydrogen evolution, *J. Am. Chem. Soc. 126*, 16988−16999.
29. Pickett, C. J., Vincent, K. A., Ibrahim, S. K., Gormal, C. A., Smith, B. E., and Best, S. P. (2003) Electron-transfer chemistry of the iron-molybdenum cofactor of nitrogenase: Delocalized and localized reduced states of FeMoco which allow binding of carbon monoxide to iron and molybdenum, *Chem. Eur. J. 9*, 76−87.
30. Liang, F. P., Jacobsen, H., Schmalle, H. W., Fox, T., and Berke, H. (2000) Carbonylhydridonitrosyltris(trimethylphosphine)molybdenum(0): An activated hydride complex, *Organometallics 19*, 1950−1962.
31. Field, L. D., Lawrenz, E. T., Shaw, W. J., and Turner, P. (2000) Insertion of CO2, CS2, and COS into iron(II)-hydride bonds, *Inorg. Chem. 39*, 5632−5638.
32. Thorneley, R. N. F., Ashby, G. A., Julius, C., Hunter, J. L., and Webb, M. R. (1991) Nitrogenase of *Klebsiella pneumoniae*—reversibility of the reductant-independent MgATP cleavage reaction is shown by MgADP catalyzed phosphate water oxygen exchange, *Biochem. J. 277*, 735−741.
33. Pickett, C. J. (1996) The Chatt cycle and the mechanism of enzymic reduction of molecular nitrogen, *J. Biol. Inorg. Chem. 1*, 601−606.
34. Thorneley, R. N. F., and Lowe, D. J. (1984a) The mechanism of *Klebsiella pneumoniae* nitrogenase action: Pre-steady-state kinetics of an enzyme-bound intermediate in N_2 reduction and of NH_3 formation, *Biochem. J. 224*, 887−894.
35. Thorneley, R. N. F., and Lowe, D. J. (1984b) The mechanism of *Klebsiella pneumoniae* action: Simulation of the dependences of H_2-evolution rate on component protein concentration and ratio and sodium dithionite concentration, *Biochem. J. 224*, 903−909.

BI050453M